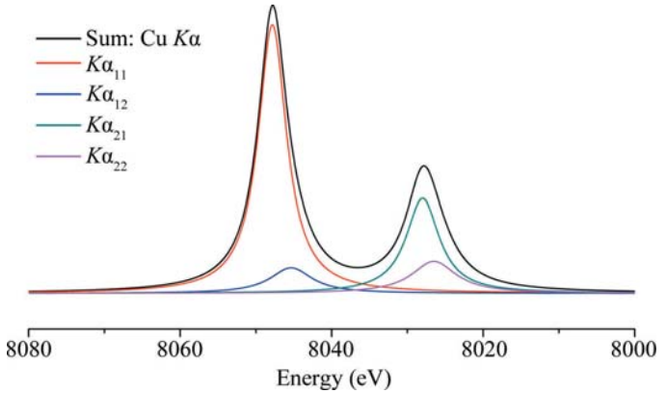

Figure 3.1.11
The emission spectrum of Cu $K\alpha$ radiation as provided by Hölzer *et al.* (1997), represented by four Lorentzian profiles: two primary ones and a pair of smaller ones to account for the observed asymmetry. The satellite lines, often referred to as the $K\alpha_3$ lines, are not displayed.

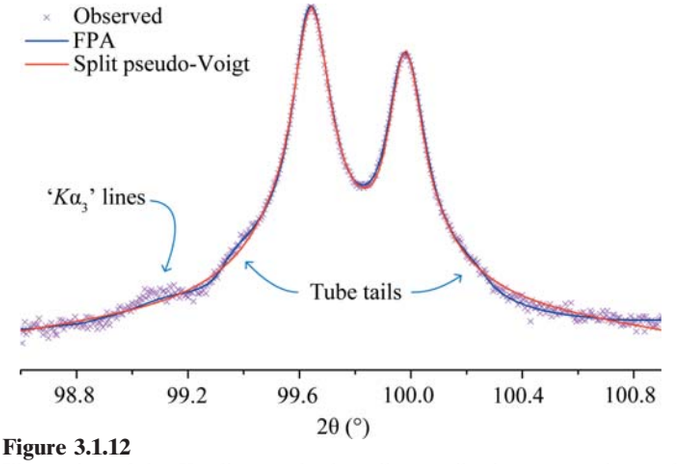

Figure 3.1.12
Illustration of the $K\alpha_3$ lines and tube-tails contributions to an observed profile on a log scale, shown with two fits: the fundamental-parameters approach, which includes these features, and the split pseudo-Voigt PSF, which does not.

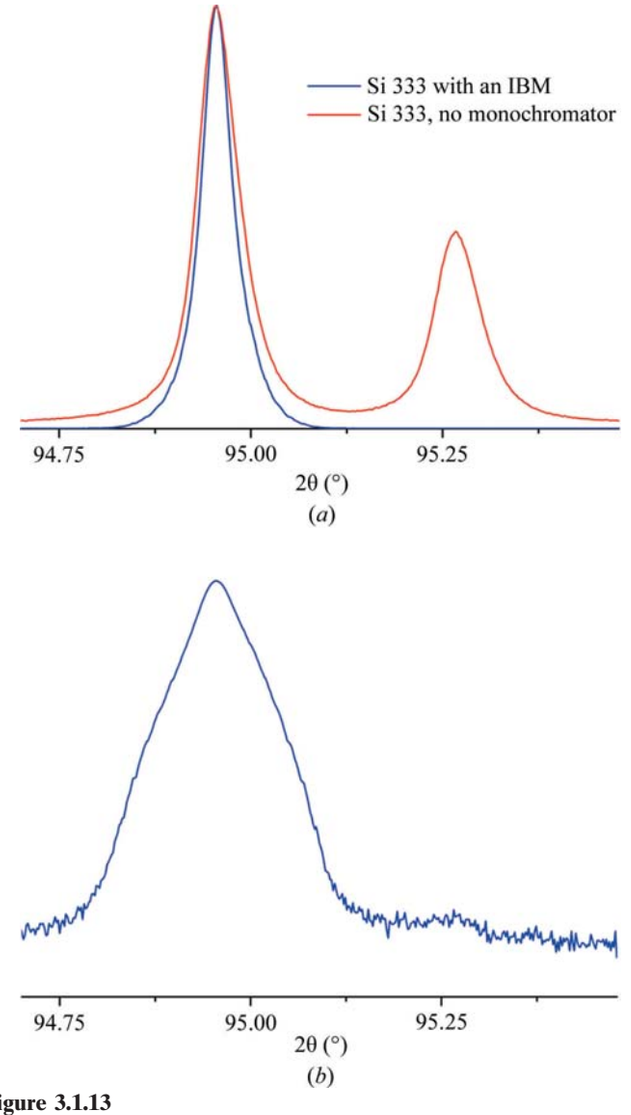

Figure 3.1.13
Illustration of the effect of the Johansson optic on the Cu $K\alpha$ emission spectrum. (*a*) Data collected for the Si 333 single-crystal reflection on a linear scale. (*b*) Analogous data from Johansson optic alone on a log scale. Both data sets were collected with 0.05 mm incident and receiving slits. The near absence of the $K\alpha_2$ scatter displayed in (*b*) can only be realized with the use of a properly aligned anti-scatter slit located at the focal line of the optic.

Bragg's law to obtain $d\theta/d\lambda$. The dominant term in the result is $\tan\theta$, which leads to the well known 'stretching' of the wavelength distribution with respect to 2θ. Maskil & Deutsch (1988) characterized a series of satellite lines in the Cu $K\alpha$ spectrum with an energy centred around 8080 eV and an intensity relative to the $K\alpha_1$ line of 6×10^{-3}. These are sometimes referred to as the $K\alpha_3$ lines, and are typically modelled with a single Lorentzian within the FPA. The 'tube tails' as reported by Bergmann *et al.* (2000) are a contribution that is strictly an artifact of how X-rays are produced in the vast majority of laboratory diffractometers. With the operation of an X-ray tube, off-axis electrons are also accelerated into the anode and produce X-rays that originate from positions other than the desired line source. They are not within the expected trajectory of para-focusing X-ray optics and produce tails on either side of a line profile as illustrated, along with the $K\alpha_3$ lines, in Fig. 3.1.12. Lastly, the energy bandpass of the pyrolytic graphite crystals used in post-monochromators is not a top-hat (or square-wave) function. Thus, the inclusion of a post-monochromator influences the observed emission spectrum.

A Johansson IBM dramatically reduces the complexity of the IPF by largely removing the $K\alpha_2$, $K\alpha_3$ and tube-tails contributions to the observed profile shape. The vast majority of the *Bremsstrahlung* is also removed. Furthermore, the inclusion of the IBM increases the path length of the incident beam by 25 to 30 cm. This substantially reduces the contribution of axial divergence to the observed profile shape. The crystals used are almost exclusively germanium (the 111 reflection), and are ground and bent to the Johansson focusing geometry, as shown in Fig. 3.1.3. They can be symmetric, with the source-to-crystal distance a and the crystal-to-focal point distance b being equal, in which case they will exhibit a bandpass of the order of 8 eV. They will slice a central portion out of the $K\alpha_1$ line, clipping the tails, to transmit perhaps 70% of the original width of the Cu $K\alpha_1$ emission spectrum. This yields a symmetric profile shape of relatively high resolution, or reduced profile breadth (other parameters being equal). The crystals can also be asymmetric, with the distance a being ~60% of the distance b. These optics will exhibit a bandpass of the order of 15 eV, in which case they transmit most of the $K\alpha_1$ line for a higher intensity, but with a lower resolution. The optic discussed here is of the latter geometry, as shown in Fig. 3.1.3.

A potential drawback to the use of an IBM concerns the nature of the $K\alpha_1$ emission spectrum it transmits, which may preclude the use of data-analysis methods that are based upon an accurate